Density Invariant Contrast Maximization for Neuromorphic Earth Observations
-Supplementary Materials-

Sami Arja [1], Alexandre Marcireau[1], Richard L. Balthazor[2], Matthew G. McHarg[2], Saeed Afshar[1] and Gregory Cohen[1]

In this document, we describe our novel dataset and provide an additional detailed explanation of our mathematical approach in the paper “Density Invariant Contrast Maximization for Neuromorphic Earth Observations”.

I. ISS Dataset

The ISS-based event camera setup consists of two DAVIS cameras, each with a resolution of 240x180 pixels, located at the Columbus module. One camera, referred to as the “Ram camera,” points forward toward the Earth’s limb in the direction of the ISS’s travel. The other camera, known as the “Nadir camera,” points down towards the Earth at a 20-degree angle to starboard to observe lightning and the Earth’s surface directly from above the upper atmosphere. The camera field-of-view (FOV) is depicted in Figure 1(a) with yellow shades representing both the Nadir and Ram FOV and the blue shade representing the ISS center FOV at its midpoint. Figure 1(b) illustrates the FOV for both cameras from the Nadir and Ram perspectives, showcasing the Ram’s zooming ability and the Nadir’s translation motion. The Ram is primarily used to observe sprites and lightning from different angles, while the Nadir captures lightning and Earth’s surface. We carefully selected ten recordings from the Nadir camera dataset, considering a variety of conditions such as weather, location, time, and noise. Table I provides additional details about each recording. We focused on recordings that exhibit rich textures and clear outlines of the Earth, disregarding recordings over the ocean, as they only generate noise without features or clear outlines, rendering them unusable.

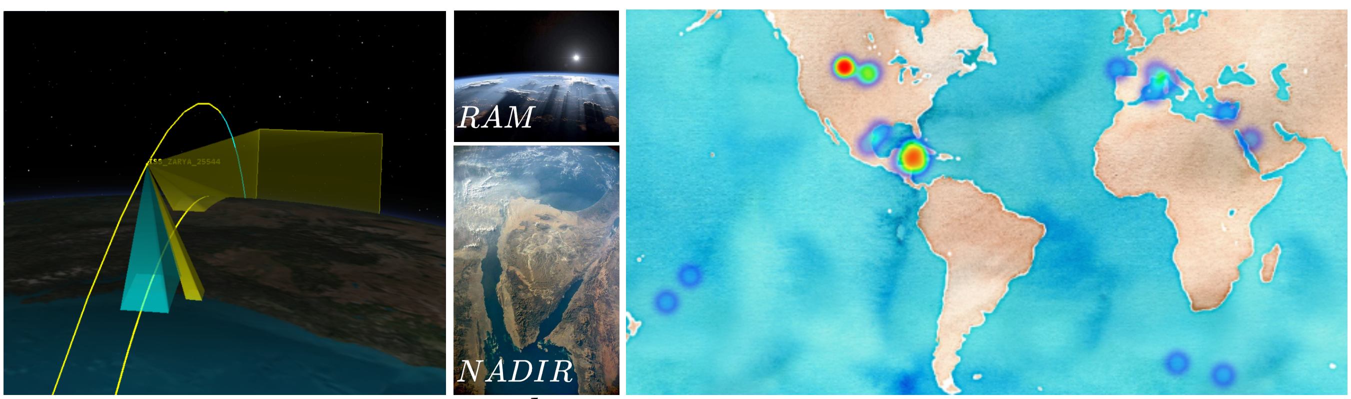

a *b* *c*

Fig. 1: The FOV of the event camera on the ISS. **a:** The yellow shade represents the FOV of two event cameras, in this work, we use the event camera pointed toward earth or NADIR. **b:** An example of what a normal camera see through the RAM and NADIR FOV. **c:** A heatmap of the recording locations which are selected for this paper.

TABLE I: General characteristics of the ISS event dataset.

Geo Location	Date (UTC)	Δt (s)	Location°	# Events	Earth Side
El Salvador	2022-01-21 20:58:34	60	15.45 -82.11	11,550,402	Day
Panama	2022-01-24 20:12:11	30	16.81 -86.61	13,876,281	Day
Brittany	2022-01-25 21:21:18	60	44.41 5.33	841,024	Night
Mexico	2022-01-25 20:58:52	90	23.16 -98.83	1,020,556	Day
Spain	2023-01-13 03:17:57	30	-0.958 36.535	3,928,491	Night

[1]S. Arja, A. Marcireau, S. Afshar, and G.Cohen are with the International Centre for Neuromorphic Systems, Western Sydney University, Australia, s.elarja at westernsydney.edu.au

[2]R. L. Balthazar and M. G. McHarg are with the U.S. Air Force Academy, Space Physics and Atmospheric Research Center, Department of Physics and Meteorology, United States Air Force Academy, Colorado, United States

TABLE I: General characteristics of the ISS event dataset.

Geo Location	**Date (UTC)**	Δt (s)	**Location°**	**# Events**	**Earth Side**
Washington	2022-02-01 20:15:58	30	43.79 -100.18	3,280,126	-
Houston	2022-02-17 20:28:02	59	20.75 -84.59	4,996,157	Night
Sumatra	2022-02-17 21:20:49	180	-48.63 13.163	1,073,675	Night
Egypt	2022-02-03 17:28:03	180	32.94 30.96	6,426,732	-
United Kingdom	2023-01-19 20:25:10	60	8.157 51.637	3,712,626	-

Below are some snapshots of each data we used in this work (Table II) with the output maps (Figure 2) which are similar to the ones presented in the paper but with a larger size:

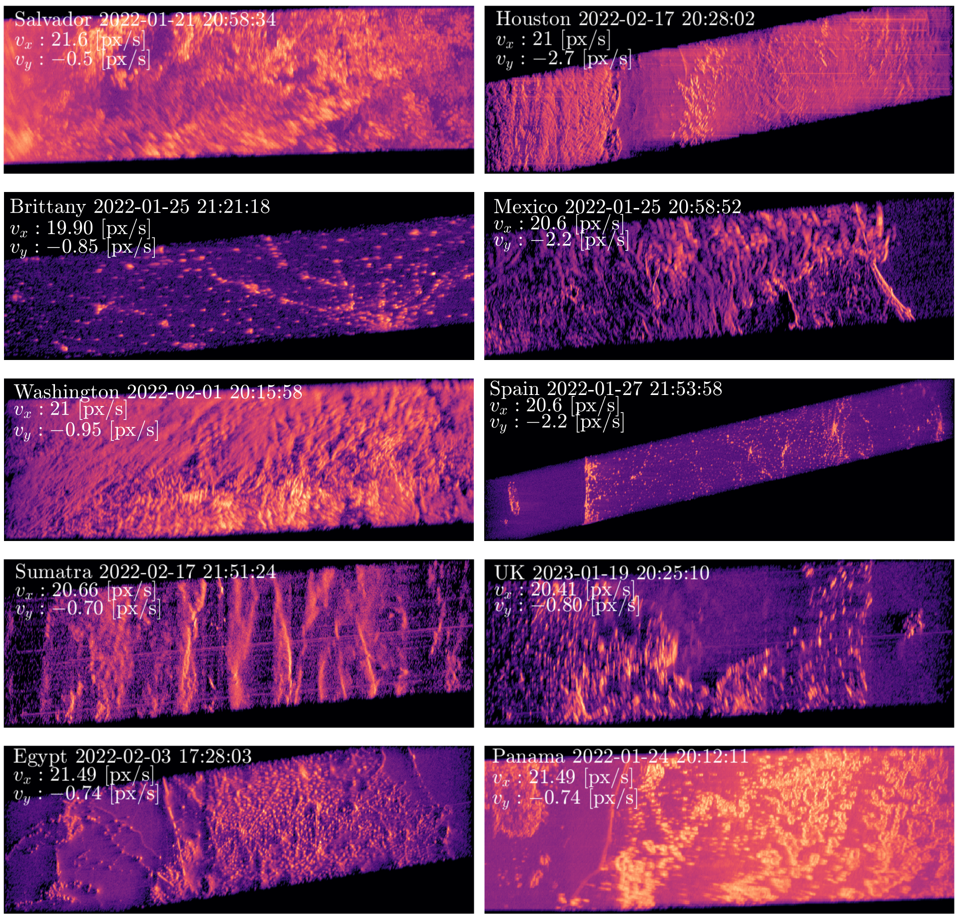

Fig. 2: Motion-compensated Maps showing details for each recording.

II. Further explanations on the One-dimensional case

In Section 2.1, we introduced the one-dimensional correction and explained the mathematical details of the continuous noise variance for condition 1. In this section, we shall explain the details of condition 2 (figure 3).

Condition 2 starts when $s \geq 1$. It is also a piecewise linear function made of three segments, however, its height is influenced by the change of the candidate speed s when it becomes larger than the pixel width. In this case, the height of the polyhedron reduces as s increases. It is described as follows:

$$f(p) = \begin{cases} \frac{cp}{s} & 0 \leq p \leq 1 \\ \frac{c}{s} & 1 \leq p \leq s \\ \frac{s-p+1}{s^2} & s \leq p \leq 1+s \end{cases} \tag{1}$$

Applying the formulas for the mean and variance given for $s \geq 1$:

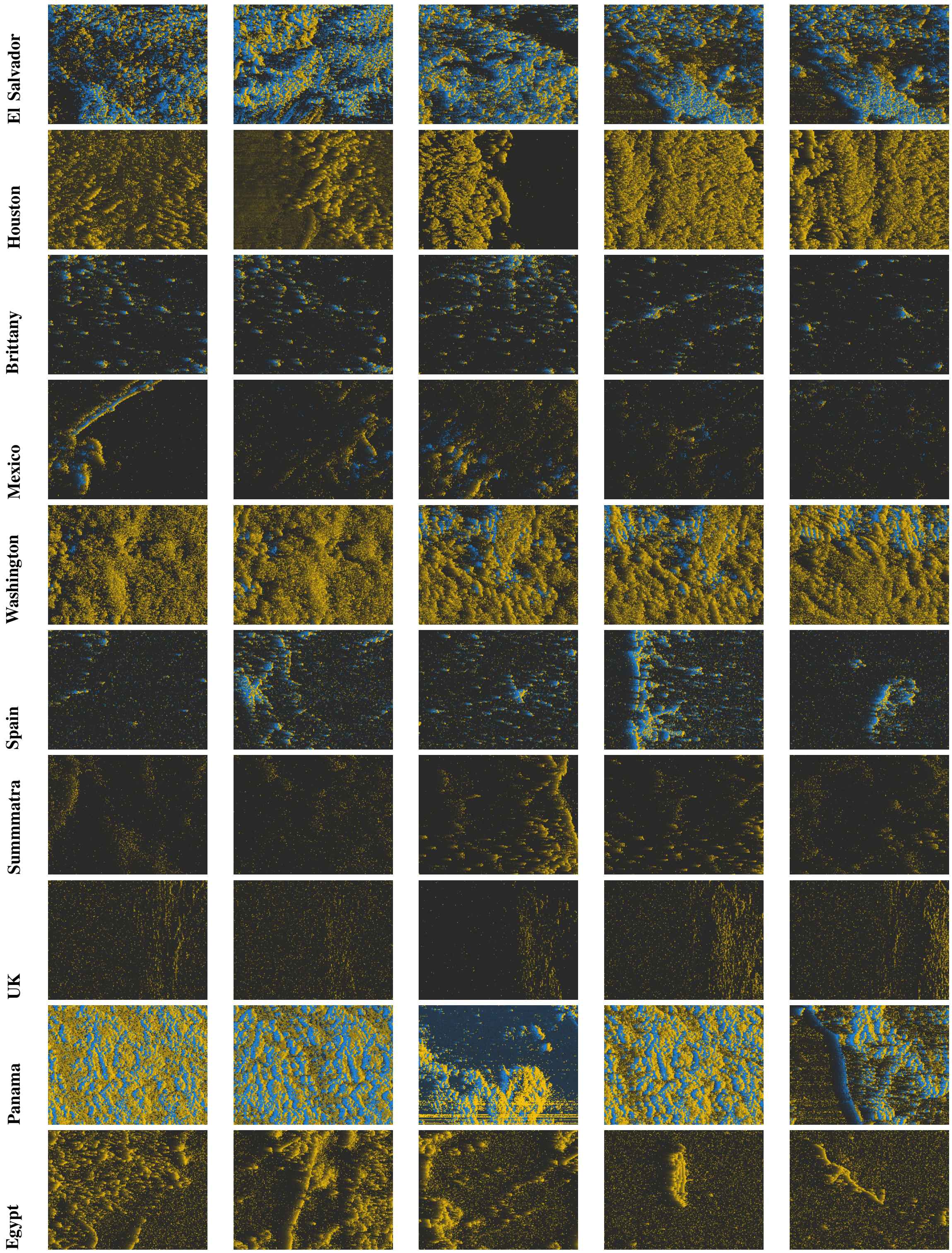

TABLE II: Frames for each dataset in sequential order.

$$\overline{f} = \frac{c}{s+1} \quad \text{and} \quad \text{var}_f(s) = c^2 \frac{s(2-s)}{3\,(s+1)^2} \tag{2}$$

$\overline{f}$ for both conditions ($s \leq 1$ and $s \geq 1$) yield the same value, showing that the consistency of the geometrical shape is preserved even at a large speed candidate. In this case, we also want var_f to be zero. We thus introduced α as a multiplicative correction function for the same non-constant segments.

$$\lambda(p) = \alpha(p) \cdot f(p) \tag{3}$$

$$\alpha(p) = \begin{cases} \frac{s}{p} & 0 \leq p \leq 1 \\ s & 1 \leq p \leq s \\ \frac{s^2}{-p+s+1} & s \leq p \leq 1+s \end{cases} \tag{4}$$

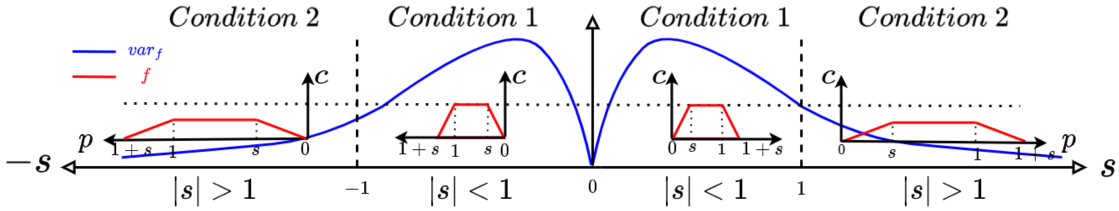

Fig. 3: The changes in the geometry of the *Line of Warped Events* f across different s.

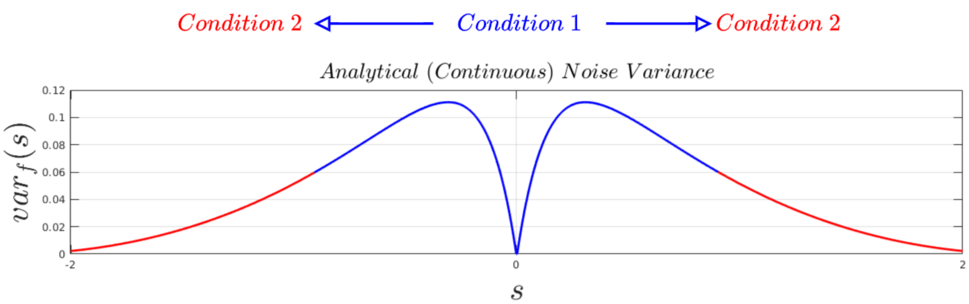

Fig. 4: Plot of the variance of f combining $var_f(s)$ for $s \leq 1$ and $s \geq 1$.

This shows that the piecewise functions for condition 1 and 2 correctly model the changes in the geometry of the proposed solid rectangle.

III. Further explanations on the Two-dimensional case

In Section 2.2, we introduced the two-dimensional correction function for $s_x \geq 1$ and $s_y \geq 1$. In this section, we shall describe the entire two-dimensional space for conditions where $s_x \leq 1$ and $s_y \leq 1$.

Similarly to the one-dimensional case, once the candidate speed is greater than the width or the height of the sensor, the height of the trapezoid will start to reduce with respect to the speed parameters. As shown in figure 5, the geometry in every condition exhibits several symmetries and can be solved by considering only two sets of conditions for conditions 2 and 3.

Therefore, we define the height function f for both for $s_x \geq 1$ and $s_y \geq 1$ as follows:

$$f(p_x, p_y) = \begin{cases} \frac{cp_y}{s_y} & p_x \leq 1 \wedge p_y \leq \frac{s_y}{s_x p_x} \\ \frac{cp_x}{s_x} & p_x \leq \frac{s_x}{s_y p_y} \wedge p_y \leq \frac{s_y}{s_x} \\ c\left(\frac{1}{s_x} - \frac{p_x}{s_x} + \frac{p_y}{s_y}\right) & 1 \leq p_x < s_x \\ & \wedge \frac{(p_x-1)s_y}{s_x} \leq p_y \leq \frac{p_x s_y}{s_x} \\ \frac{cp_x}{s_x} & p_x \leq 1 \wedge \ \frac{s_y}{s_x} \leq p_y \leq 1 \\ \frac{c}{s_x} & 1 \leq p_x \leq s_x \\ & \wedge \ \frac{p_x s_y}{s_x} \leq p_y \leq \frac{(p_x-1)s_y}{s_x+1} \\ c\left(\frac{1}{s_x} - \frac{p_x}{s_x} + \frac{p_y}{s_y}\right) & s_x \leq p_x \leq 1 + s_x \\ & \wedge \ \frac{(p_x-1)s_y}{s_x} \leq p_y \leq s_y \end{cases} \tag{5}$$

Due to the consistent symmetry, calculating the mean of f yields a similar value to condition 1:

$$\overline{f} = \frac{c}{s_x + s_y + 1} \tag{6}$$

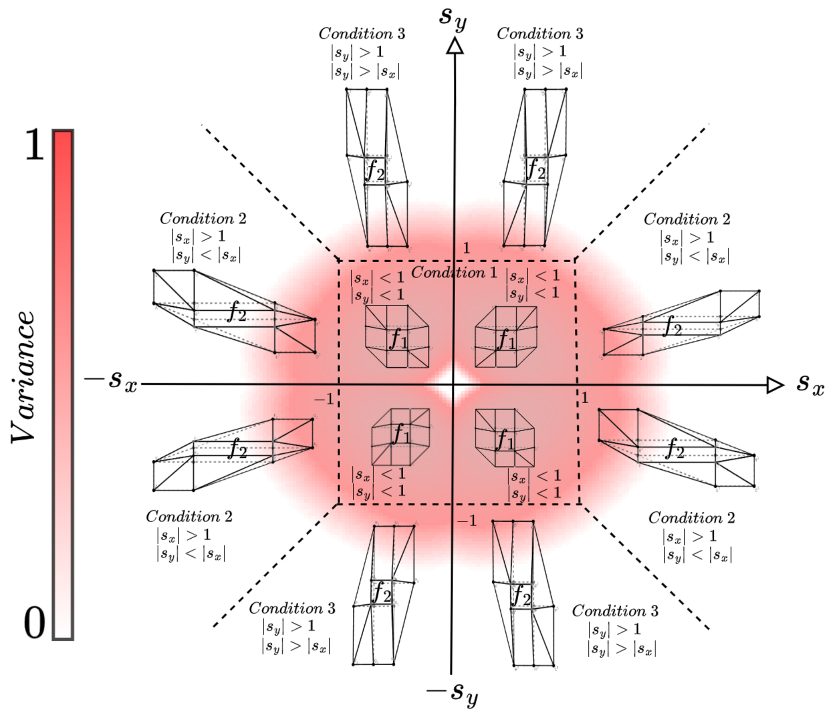

Fig. 5: An illustration of the height of the sheared rectangular cuboid (accumulated warped events) as a function of s_x and s_y (black geometric figures) and the corresponding variance (red and white background). The problem exhibits several symmetries and can be solved by considering only two sets of conditions (condition 2 and condition 3 are symmetrical about the axis $y = x$).

$$\text{var}_f(s_x, s_y) = \frac{c^2\left(4s_x^2 s_y + 4s_x^2 - 2s_x s_y^2 - 3s_x s_y - 2s_x + s_y^2 + s_y\right)}{6s_x^3\left(s_x + s_y + 1\right)^2} \tag{7}$$

To cancel out the effect of noise variance, we introduce α that is specific to f with the same properties as the previously introduced α. That's to be multiplicative and flatten f to ensure that the variance of the corrected height function is zero.

$$\alpha(p_x, p_y) = \begin{cases} \frac{s_y}{p_y} & p_x \leq 1 \wedge p_y \leq \frac{s_y}{s_x p_x} \\ \frac{s_x}{p_x} & p_x \leq \frac{s_x}{s_y p_y} \wedge p_y \leq \frac{s_y}{s_x} \\ \frac{s_x s_y}{s_x p_y - s_y p_x + s_y} & 1 \leq p_x < s_x \\ & \wedge \frac{(p_x - 1) s_y}{s_x} \leq p_y \leq \frac{p_x s_y}{s_x} \\ \frac{s_x}{p_x} & p_x \leq 1 \wedge \ \frac{s_y}{s_x} \leq p_y \leq 1 \\ s_x & 1 \leq p_x \leq s_x \\ & \wedge \ \frac{p_x s_y}{s_x} \leq p_y \leq \frac{(p_x - 1) s_y}{s_x + 1} \\ \frac{s_x s_y}{s_x p_y - s_y p_x + s_y} & s_x \leq p_x \leq 1 + s_x \\ & \wedge \ \frac{(p_x - 1) s_y}{s_x} \leq p_y \leq s_y \end{cases} \tag{8}$$

In figure 6, we compared the output variance using the analytical formula as a function of the candidate speed and the discrete simulated noise. Both show an exact match.

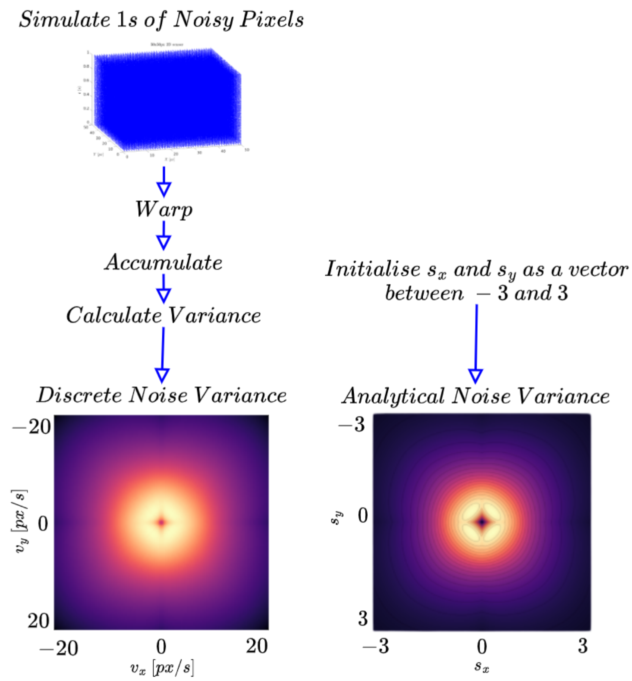

Fig. 6: Comparison of the variance results between both analytical and discrete variance equation. The discrete analytical variance was performed by simulating dense noise events of dimension 50×50 pixels, while the analytical variance was calculated using $\mathrm{var}_f(s_x, s_y)$.